

Quantum-Spillover Enhanced Surface-Plasmonic Absorption at the Interface of Silver and High-Index Dielectrics

Dafei Jin,¹ Qing Hu,¹ Daniel Neuhauser,² Felix von Cube,³ Yingyi Yang,¹
Ritesh Sachan,⁴ Ting S. Luk,⁵ David C. Bell,³ and Nicholas X. Fang^{1,*}

¹Department of Mechanical Engineering, Massachusetts Institute of Technology, Cambridge, Massachusetts 02139, USA

²Department of Chemistry and Biochemistry, University of California at Los Angeles, Los Angeles, California 90095, USA

³School of Engineering and Applied Sciences, Harvard University, Cambridge, Massachusetts 02138, USA

⁴Materials Science and Technology Division, Oak Ridge National Laboratory, Oak Ridge, Tennessee 37831, USA

⁵Sandia National Laboratory, Albuquerque, New Mexico 87123, USA

(Dated: April 30, 2015)

We demonstrate an unexpectedly strong surface-plasmonic absorption at the interface of silver and high-index dielectrics. We show, from first-principles, that due to the lowered metal-to-dielectric work-function at such interface, conduction electrons display a drastic quantum spillover, causing the interfacial electron-hole pair production to become the predominant dissipation channel. The theoretical prediction is supported experimentally by the electron-energy loss spectroscopy and ultraviolet-visible spectrophotometry. This finding can be of fundamental importance in understanding and designing quantum nano-plasmonic devices, which utilize metal-high-index contacts.

PACS numbers: 42.79.Wc, 73.20.Mf, 78.20.-e, 78.68.+m

Surface plasmons (SPs), collective oscillations of conduction electrons at a metal-dielectric interface, have attracted interest for several decades [1–3]. Nanomaterials that strongly absorb visible light through plasmonic effects could be very important for solar-energy devices [4–8]. It is normally assumed that classical theory, with prescribed frequency-dependent bulk permittivities, reliably captures the SP properties. Quantum effects, despite their academic interest [9–13], are usually considered to have negligible effect in practical systems.

Here we show, however, that contrary to conventional wisdom, quantum effects can play a crucial role for SPs at the interface of silver (Ag) and (practically any) high-index dielectrics. Our density-functional calculations and spectroscopic measurements demonstrate the existence of remarkable non-classical plasmonic absorption in such systems. We show that the predominant decay channel of SPs turns out to be the interfacial electron-hole (e-h) pair production [2, 14–18], as opposed to ordinary phonon scattering (the Drude loss) or interband transitions (the dielectric loss). Our results underscore the quantum origin of this plasmonic absorption that has been largely overlooked in the nano-plasmonics community.

High-index dielectrics have been long considered as superior gate insulators in nano-electronics [19]. They are capable of boosting the charge mobility in nanostructured semiconductor transistors by screening the Coulombic charged-impurity scattering [20]. In the recent years, they have also attracted much interest in nanophotonics on the conversion of SPs to hot electrons [5, 21–24]. However, very limited attention has been paid to their quantum electronic properties that can reversely modify the SP response. The uniqueness of high-index dielectrics, compared with low-

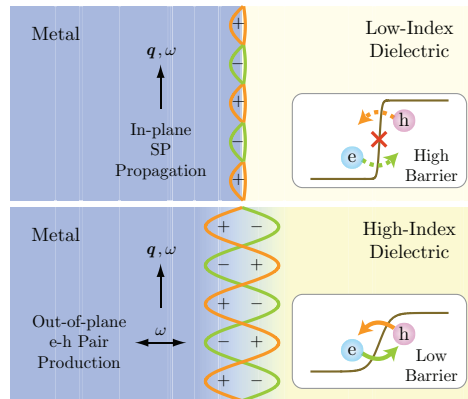


FIG. 1: Schematics for the coupling of surface plasmons and interfacial electron-hole pairs at the interface of a metal and low-index or high-index dielectric. Low barriers yield wider interfacial regions where electrons and holes coexist and can couple to the propagating SPs.

index dielectrics (including vacuum and air), lies in their large electron affinity, high static permittivity, and thereby a much lowered work-function to the conduction electrons in metal. This allows the electrons to undergo a deep quantum spillover into the high-index dielectrics extending beyond the Thomas-Fermi screening length. Consequently, the in-plane SP propagation strongly couples with the out-of-plane e-h pair production, which drastically intensifies the energy dissipation and broadens the absorption spectrum. The e-h pair production can be viewed intuitively as dipole transitions across the interface driven by the out-of-plane electric field of SPs, as illustrated in Fig. 1. This process is insignificant at metal-low-index contacts [2, 14, 15] due to the high barrier and thus insufficient quantum

spillover. Nevertheless, as demonstrated in this paper, it is remarkable at Ag-high-index contacts and can lead to useful applications for quantum nano-plasmonic devices.

Our theoretical study is based on a jellium density-functional model that we generalize to incorporate the most crucial properties of Ag and dielectrics. An Ag slab, uniform in x - y , with a thickness of $d = 100 a_0$ (a_0 is the Bohr radius) along z , is clamped by a dielectric on both sides (see the inset of Fig. 2). The conduction electrons are governed by the Kohn-Sham equations and generalized Poisson equation [25–29],

$$\left\{ -\frac{\hbar^2}{2m} \frac{d^2}{dz^2} + V_{\text{eff}}[n_-(z)] \right\} \varphi_\nu(z) = \varepsilon_\nu \varphi_\nu(z), \quad (1)$$

$$\frac{d}{dz} \left\{ \epsilon(z; \omega) |_{\omega \rightarrow 0} \frac{d}{dz} \Phi(z) \right\} = 4\pi e \{ n_-(z) - n_+(z) \}. \quad (2)$$

$\varphi_\nu(z)$ and ε_ν are the eigenfunctions and eigenvalues. $n_-(z)$, the electron number density, is a weighted sum of $|\varphi_\nu(z)|^2$ over the occupied orbitals up to the Fermi level μ_F [28, 29]. $n_+(z)$ is the space-dependent positive-jellium density; $\epsilon(z; \omega)$ is the space- and frequency-dependent background permittivity introduced to account for the screening by valance electrons. The effective potential $V_{\text{eff}}[n_-(z)]$ reads

$$V_{\text{eff}}[n_-(z)] = -e\Phi(z) + V_{\text{xc}}[n_-(z)] + \alpha(z), \quad (3)$$

where $V_{\text{xc}}[n_-(z)]$ is the exchange-correlation potential, and $\alpha(z)$ is the space-dependent electron affinity in a flat-band picture [30]. A general Green's function $\mathcal{G}(z, z'; q; \omega)$ for this layered system is derived, and used in conjunction with the Poisson equation for both the statics (in-plane wavenumber $q \rightarrow 0$ and frequency $\omega \rightarrow 0$) and dynamic response. (See Supplemental Material for details.)

Several high-index dielectrics, Al_2O_3 , HfO_2 , and TiO_2 , are investigated; and for comparison, the medium- and low-index dielectrics, SiO_2 and air are included. Table I lists the material properties used and obtained in our calculation. Figure 2 shows the near-interface ground-state electron density profile $n(z)/\bar{n}$ and effective potential $V_{\text{eff}}(z)$. With increasing static permittivity and electron affinity, the Friedel oscillation gradually vanishes and the potential barrier (work-function) drops by as much as 2 eV. An increasing number of electrons spill from Ag into the dielectrics. This behavior can be quantified by a characteristic spillover depth, $\zeta \equiv \int_0^{+\infty} dz n_-(z)/\bar{n}$, which represents the distance up to which the spilled density would extend if it had the constant bulk value \bar{n} [2, 15]. As shown in Table I, ζ of HfO_2 or TiO_2 is 2 to 3 times greater than that of air, and has approached the Thomas-Fermi screening length, $l_{\text{TF}} \approx 0.58 \text{ \AA}$ of Ag. The actual density tail penetrates several times further, as shown in Fig. 2. This is the key feature leading to the intrinsic spectral broadening of SPs on a Ag-high-index contact.

TABLE I: Adopted material constants of the dielectrics [19, 31–36]: electronic bandgap E_g , electron affinity α_D , permittivity in statics $\epsilon_{D0} \equiv \epsilon_D(\omega \rightarrow 0)$, and permittivity at 532 nm optical frequency $\epsilon_D(\omega_{532})$. Calculated Ag-to-dielectric work function W and spillover depth ζ .

Material	E_g (eV)	α_D (eV)	ϵ_{D0}	$\epsilon_D(\omega_{532})$	W (eV)	ζ (\text{\AA})
Air	“ ∞ ”	0	1	1	4.26	0.18
SiO_2	9.0	0.95	3.9	2.13	3.22	0.24
Al_2O_3	8.8	1.70	9.0	3.13	2.73	0.32
HfO_2	5.8	2.14	25.0	4.33	2.47	0.39
TiO_2	3.2	3.00	86.0	6.55	2.26	0.58

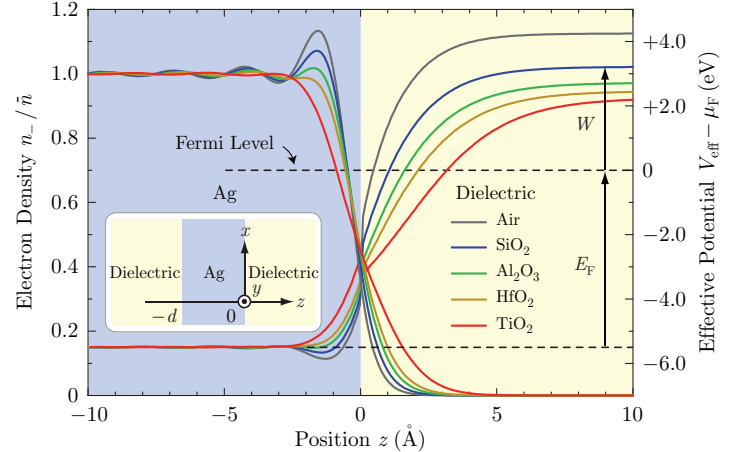


FIG. 2: Calculated ground-state electron-density profiles and effective-potential profiles. The potential is plotted with respect to the Fermi level μ_F .

To understand the dynamics of spillover-induced damping, and to compare it with the experiment, we use a time-dependent linear-response calculation [28, 37]. The system-mediated effective interaction between two external charge sheets at Z and Z' is [37]

$$\mathcal{W}(Z, Z', q; \omega) = \int dz dz' \mathcal{G}(Z, z, q; \omega) \times \chi(z, z', q; \omega) \mathcal{G}(z', Z', q; \omega), \quad (4)$$

where $\chi(z, z', q; \omega)$ is the susceptibility. (See Supplemental Material.) The surface response function, $g(q; \omega) \equiv (q/2\pi)\epsilon_D(\omega)\text{Im}\mathcal{W}(Z_0, Z_0, q; \omega)$ describes the amplitude of surface excitations caused by an external charge sheet at Z_0 , which we take to be $50 a_0$ outside the Ag [2].

Figure 3(a) gives the calculated $g(q; \omega)$ at a representative wavenumber $q = 0.05 a_0^{-1}$, which amounts to a 6.6 nm wavelength, a typical length scale relevant to both optical and electronic excitations. The main peaks in Fig. 3(a) correspond to the SP excitations. As the dielectric index rises, they change from a narrow 3.57 eV resonance for air to a broad feature around 2.51 eV for TiO_2 . Note that the spectral broadening

(and the associated damping) here takes place *without* phonon scattering or interband transitions, as the model does not have these loss channels. Further, Fig. 3(b), which displays the induced density variation (scaled by ϵ_D for clarity) corresponding to each peak frequency, confirms these modes to be surface modes localized at the interface.

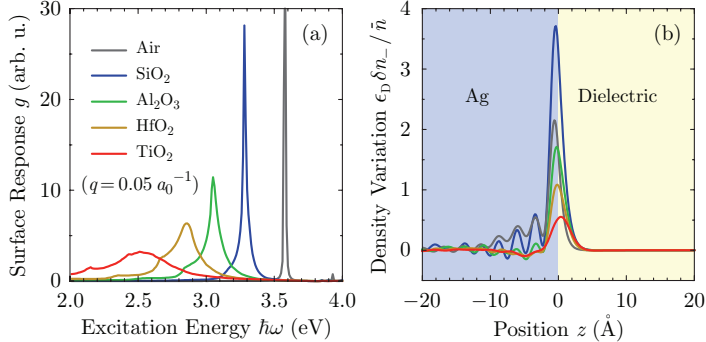


FIG. 3: Calculated dynamic surface response (a) and induced density variation (b). The in-plane wavenumber is $q = 0.05 a_0^{-1}$.

The intrinsic dissipation mechanism responsible for the enhanced SP decay is the interfacial e-h pair production as shown in Fig. 1. On a usual metal-vacuum jellium contact, the decay rate of SPs through e-h pairs at long wavelengths is proportional to the imaginary part of the Feibelman parameter d_{\perp} . It is related to the spillover depth ζ by a sum rule [15], $\text{Im} \int_0^{\infty} d\omega \omega d_{\perp}(\omega) = \frac{\pi}{2} \omega_p^2 \zeta$, where ω_p is the bulk-plasmon frequency. Obviously, a classical theory with $\zeta \equiv 0$ cannot produce any out-of-plane e-h pairs. For metal-low-index contacts, ζ is often too small to activate this dissipation channel. Consequently, only for metal-high-index contacts with an appreciable ζ (refer to Table I), e-h pair production can become the predominant dissipation channel, exceeding the ordinary phonon scattering and interband transitions.

To be specific, we calculate the energy-momentum loss spectrum $\Gamma(\mathbf{q}, \omega)$ for a high-energy electron penetrating through the system. It reads [37, 38]

$$\begin{aligned} \Gamma(\mathbf{q}, \omega) = & -C \int dZ dZ' \cos \left[\frac{\omega}{v_{\text{in}}} (Z - Z') \right] \\ & \times \text{Im} \mathcal{W}(Z, Z', q; \omega), \end{aligned} \quad (5)$$

where C is a universal constant and v_{in} is the incoming velocity of the electron (80 keV in our calculation and experiment). We compare the calculated $\Gamma(\mathbf{q}, \omega)$ between an actual HfO_2 and a *fictitious* HfO_2 . The latter shares the same SP frequency location with the *actual* HfO_2 , but possesses the ground-state properties of air (not HfO_2). We can then differentiate how distinct ground-state behaviors influence the SP excitation.

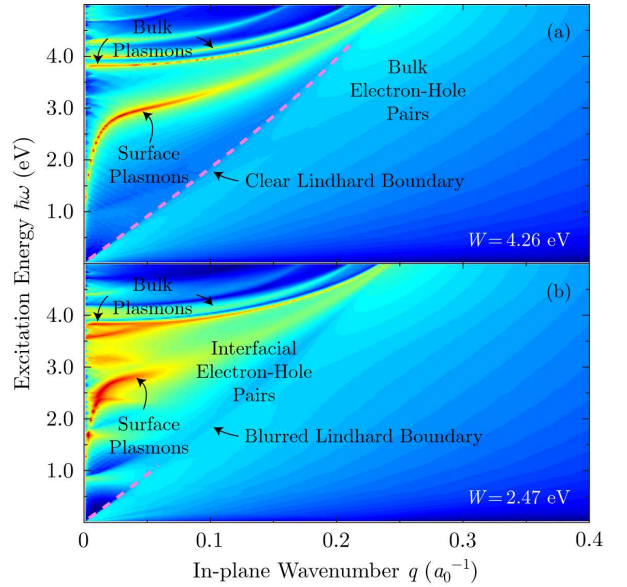


FIG. 4: Calculated energy-momentum loss spectrum $\Gamma(\mathbf{q}, \omega)$ plotted in logarithmic scale. Red means high loss and blue means low loss. (a) For a *fictitious* HfO_2 with an Ag-to-dielectric work-function $W = 4.26 \text{ eV}$. (b) For an *actual* HfO_2 with an Ag-to-dielectric work-function $W = 2.47 \text{ eV}$ (refer to Table I). Note that for a $100 a_0$ thin Ag slab in our model, there are more than one bulk-plasmon curves shown on the spectra.

Figures 4(a) and (b) give the calculated results. As can be seen, the SP resonance for the *fictitious* HfO_2 ($W = 4.26 \text{ eV}$) is much sharper than for the *actual* HfO_2 ($W = 2.47 \text{ eV}$). Fig. 4(a) displays a clear boundary, which we term as the Lindhard boundary [39], between the SP resonance and the bulk e-h pair production. SPs cannot decay into these bulk e-h pairs because of the energy-momentum mismatch (until Landau damping occurs at very large momentum and energy beyond our interest). In contrast, Fig. 4(b) displays a thoroughly blurred region between the SP resonance and the bulk e-h pair region. This is the region of the interfacial e-h pair production. Since there is no energy-momentum mismatch in the z -direction (due to the broken symmetry), the electrons can actively move out-of-plane irrespective of how small q is. This explains why a ground state with a deeper quantum spillover shows a larger SP decay in the optical regime.

Experimentally, we perform an electron energy-loss spectroscopy (EELS) measurement (aberration corrected Zeiss Libra transmission electron microscope (TEM)). The acceleration voltage of the microscope is set to 80 kV, which permits an excellent energy resolution of 120 meV (FWHM of the zero-loss peak). We e-beam evaporate 20 nm Ag and 20 nm varied dielectrics sequentially onto carbon-supported TEM grids. Figure 5 gives the obtained energy-loss spectra. The broad peaks in the range of 1.5 to 1.8 eV for all dielectrics come from the

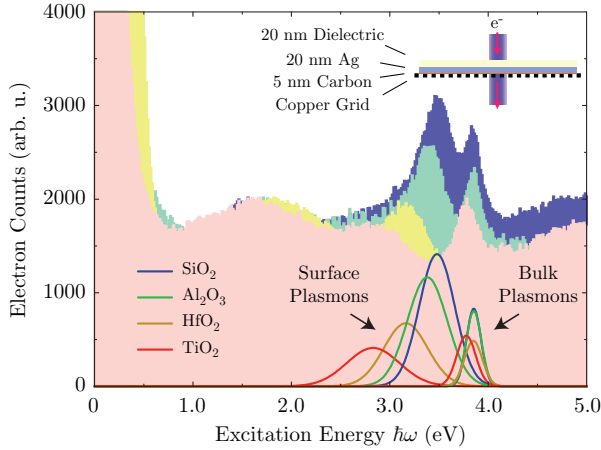


FIG. 5: Electron energy-loss spectra for 20 nm dielectrics on 20 nm silver. The incident electrons are set to 80 keV. The colored column plots display the electron counts. The colored curves show the peaks via the standard multi-Lorentzian fitting (after subtracting the zero-loss peak).

contact between 5 nm amorphous carbon and Ag [40]. These peaks are not of interest to us. The sharp peaks around 3.8 eV for all dielectrics are the bulk-plasmon resonances inside Ag [41]. The varied peaks consistently moving from 3.48 eV for SiO_2 , to 3.38 eV for Al_2O_3 , 3.16 eV for HfO_2 , and 2.83 eV for TiO_2 are the SP resonances at the Ag-dielectric interfaces. Noteworthily, there is a clear trend that, with increasing index of the dielectrics, the peak width gradually broadens. This trend signifies an enhanced damping and shortened lifetime of the SPs near the interface, in agreement with our theoretical prediction in Figs. 3 and 4. By comparison, the bulk-plasmon resonances, which decay primarily through phonon scattering (the Drude loss) and bulk e-h pair production (the Landau damping at short wavelengths) are much less affected by the varied dielectrics, as shown in Fig. 5. This fact again testifies to the increasingly dominant role of interfacial e-h pair production for SPs, with increasing index of the dielectrics.

The most striking observation is on the optical measurement with ultraviolet-visible (UV-Vis) spectrophotometry (Varian Cary 500). We first e-beam evaporate 200 nm high-quality Ag films onto ultra-smooth (roughness less than 1 nm) Pyrex glass substrates, and then deposit 20 nm varied dielectrics on Ag. We perform normal-incidence reflection measurement. (See Supplemental Material for details.) It is known that in the wavelength range of 400 to 700 nm, a 200 nm Ag film works as a perfect reflector, and our dielectrics are transparent (refer to the bandgap E_g in Table I). We would expect to see close to 100% reflectance; there should be no evanescent SPs being excited due to the momentum mismatch [1, 3]. However, as shown in Fig. 6, strong and broadband

absorption can be clearly observed around the SP resonance of each dielectrics. The absorption intensifies with increasing index of the dielectrics. To ensure that the loss is not caused by any unknown defects or interband transitions in the dielectrics [42, 43], we have done separate transmission measurement, for the same-deposited dielectrics directly on Pyrex glass (without Ag). We indeed verify that the dielectric films themselves are lossless in the spectral range of interest, and our theoretically calculated transmittance, using the standard Sellmeier formula and Forouhi-Bloemberg formula for $\epsilon_D(\omega)$ [31, 33], agrees very well with the measurement. (See Supplemental Material.)

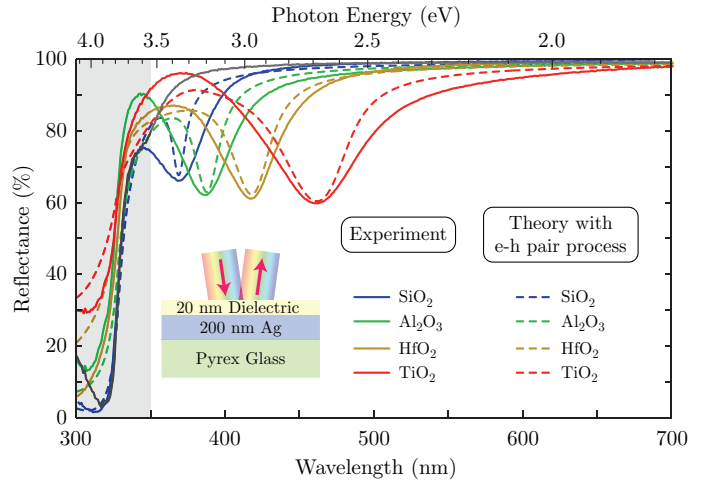


FIG. 6: Experimentally measured and theoretically calculated (including the e-h pair process) reflection spectra for 20 nm dielectrics on 200 nm silver. The grey curve is the measured reflectance of the bare 200 nm silver as a reference. The shaded region ($\lambda < 350$ nm) is where 200 nm silver is no longer a good reflector (near bulk-plasmon absorption).

In order to understand the experiment, we should first note that, owing to the unavoidable surface roughness which provides a nonzero excitation efficiency, SP absorption under normally incident light is not impossible. The so-called reflection deficit anomaly (RDA) exactly refers to such a situation [1, 44–47]. However, the main question is quantitatively how large this effect can be. We have done a careful atomic force microscope (AFM) measurement to our Ag films. It gives a root-mean-square (RMS) roughness $\delta \approx 1.1$ nm and a Gaussian-fitted correlation length $\sigma \approx 25$ nm. These numbers indicate a very smooth surface. We then perform a classical statistical-roughness calculation following Kretschmann *et al.* [46, 47]. The classical calculation cannot produce sensible agreement with the experiment. (See Supplemental Material.)

It is impractical to use the jellium model to directly compute the quantum-spillover enhanced SP absorption on a rough surface. Instead, we seek a more feasible approach by incorporating the semi-microscopic d_\perp

parameter into the statistical-roughness model. d_{\perp} measures the strength of the interfacial e-h pair process [2, 14–16], and can (phenomenologically) connect the first-principles description to the optical calculation. (See Supplemental Material for details.) Our calculated results are given by the dotted lines in Fig. 6. Even a small d_{\perp} can dramatically enhance the absorption around SP resonances. In principle, the d_{\perp} description only works accurately for long wavelengths, and it can have a strong frequency-dependence [2, 14–16], while we merely use single-valued d_{\perp} here. That explains why our fitting looks better at longer wavelengths and lower frequencies (TiO_2 and HfO_2), compared with shorter wavelengths and higher frequencies (Al_2O_3 and SiO_2). But the main trend of an increasing absorption with increasing index of the dielectrics (due to the increased e-h pair production enclosed in d_{\perp}) is still quite clear.

To summarize, we find that high-index thin films in contact with silver exhibit remarkably enhanced non-classical surface-plasmon absorption. Our first-principles calculation suggests that due to the significant quantum spillover of conduction electrons across the interface, the electron-hole pair production serves as the major dissipation channel, which can highly efficiently damp surface plasmons. This quantum-electronic behavior of the static dielectric environment to the optical excitations on metal surfaces brings on new applications in nanoscale light confinement, and new insights in surface-plasmon to hot-electron conversion.

DJ, QH, YY, and NXF acknowledge the financial support by the NSF (Award No. CMMI-1120724) and AFOSR MURI (Award No. FA9550-12-1-0488). DN acknowledges support by the NSF (Grant CHE-1112500). FvC acknowledges support by the STC Center for Integrated Quantum Materials and NSF (Grant No. DMR-1231319). DJ wish to thank Patrick. A. Lee, Fan Wang, Miguel A. Méndez Polanco, and Alexie M. Kolpak for helpful discussion.

* Electronic address: nicfang@mit.edu

- [1] H. Raether, *Surface Plasmons on Smooth and Rough Surfaces and on Gratings* (Springer, Berlin, 1988).
- [2] A. Liebsch, *Electronic excitations at metal surfaces* (Plenum Press, New York, 1997).
- [3] S. A. Maier, *Plasmonics: Fundamentals and Applications* (Springer, New York, 2007).
- [4] S. Linic *et al.*, *Nature Mater.* **10**, 911 (2011).
- [5] C. Clavero, *Nature Photonics* **8**, 95 (2014).
- [6] N. Liu *et al.*, *Nano Lett.* **10**, 2342 (2010).
- [7] K. Aydin *et al.*, *Nature Commun.* **2**, 517 (2011).
- [8] Y. Cui *et al.*, *Nano Lett.* **12**, 1443 (2012).
- [9] K. J. Savage *et al.*, *Nature* **491**, 574 (2012).
- [10] R. Esteban, A. G Borisov, P. Nordlander, and J. Aizpurua, *Nat. Commun.* **3**, 825 (2012).
- [11] G. Toscano, *et al.*, arXiv:1408.5862.
- [12] J. M. McMahon, S. K. Gray, and G. C. Schatz, *Phys. Rev. Lett.* **103**, 097403 (2009).
- [13] A. Wiener *et al.*, *Nano. Lett.* **12**, 3308 (2012).
- [14] P. J. Feibelman, *Prog. Surf. Sci.* **12**, 287 (1982).
- [15] B. N. J. Persson and E. Zarembo, *Phys. Rev. B* **31** 1863 (1985).
- [16] K. Kempa and W. L. Schaich, *Phys. Rev. B* **34** 547 (1986).
- [17] M. Rocca, *Surf. Sci. Rep.* **22**, 1 (1995).
- [18] X. Li, D. Xiao, and Z. Zhang, *New J. Phys.* **15** 023011 (2013).
- [19] J. Robertson, *Rep. Prog. Phys.* **69**, 327C396 (2006).
- [20] D. Jena and A. Konar, *Phys. Rev. Lett.* **98**, 136805 (2007).
- [21] M. L. Brongersma, Y. Cui, and S. Fan, *Nature Mater.* **13**, 451-460 (2014).
- [22] Y. K. Lee *et al.*, *Nano. Lett.* **11**, 4251 (2011).
- [23] H. Lee *et al.*, *J. Phys. Chem. C* **118**, 5650 (2014).
- [24] J. S. DuChene *et al.*, *Angew. Chem. Int. Ed.* **53**, 7887 (2014).
- [25] N. D. Lang and W. Kohn, *Phys. Rev. B* **1**, 4555 (1970).
- [26] N. D. Land and W. Kohn, *Phys. Rev. B* **3**, 1215 (1971).
- [27] A. Liebsch, *Phys. Rev. Lett.* **71**, 145 (1993).
- [28] Z. Yuan and S. Gao, *Phys. Rev. B* **73**, 155411 (2006).
- [29] Y. Gao and D. Neuhauser, *J. Chem. Phys.* **137**, 074113 (2012).
- [30] Z. Zhang and J. T. Yates, Jr., *Chem. Rev.* **112**, 5520 (2012).
- [31] E. D. Palik, *Handbook of Optical Constants of Solids* (Academic Press, New York, 1998).
- [32] F. A. Grant, *Rev. Mod. Phys.* **31**, 646 (1959).
- [33] S. Tanemura *et al.*, *Appl. Surf. Sci.* **212**, 644 (2003).
- [34] W. Zheng and K. H. Bowen, Jr., *J. Phys. Chem. A*, **109**, 11521 (2005).
- [35] F. Zhang *et al.*, *J. Mater. Chem.*, **19**, 2771 (2009).
- [36] D. O. Scanlon *et al.*, *Nat. Mater.* **12**, 798 (2013).
- [37] F. J. García de Abajo, *Rev. Mod. Phys.* **82**, 209 (2010).
- [38] D. Pines and P. Nozières, *Theory Of Quantum Liquids: Normal Fermi Liquids* (Perseus Books, Cambridge, 1999).
- [39] G. F. Giuliani and G. Vignale, *Quantum Theory of the Electron Liquid* (Cambridge University Press, New York, 2005).
- [40] J. Robertson and E. P. O'Reilly, *Phys. Rev. B* **35**, 2946 (1987).
- [41] K. Andersen, K. W. Jacobsen, and K. S. Thygesen, *Phys. Rev. B* **86**, 245129 (2012).
- [42] D. Liu *et al.*, *Appl. Phys. Lett.* **96**, 032905 (2010).
- [43] J. L. Gavartin *et al.*, *Appl. Phys. Lett.* **89**, 082908 (2006).
- [44] S. N. Jasperson and S. E. Schnatterly, *Phys. Rev.* **188**, 759 (1969).
- [45] J. M. Elson and R. H. Ritchie, *Phys. Rev. B* **4**, 4129 (1971).
- [46] E. Kröger and E. Kretschmann, *Z. Physik* **237**, 1 (1970).
- [47] E. Kretschmann and E. Kröger, *J. Opt. Soc. A.* **65**, 150 (1975).